Screen-printed electroluminescent lamp modified with graphene oxide as a sensing device

Abdulhadee Yakoh[a,b], Ruslan Álvarez-Diduk[a], Orawon Chailapakul[b,c], Arben Merkoçi[a,d]*.*

[a] Nanobioelectronics and Biosensor Group, Catalan Institute of Nanoscience and Nanotechnology (ICN2), CSIC. The Barcelona Institute of Science and Technology, Campus UAB, Bellaterra, 08193, Barcelona, Spain.

[b] Electrochemistry and Optical Spectroscopy Center of Excellence (EOSCE), Department of Chemistry, Faculty of Science, Chulalongkorn University, 254 Phayathai Road, Patumwan, Bangkok 10330, Thailand

[c] Center for Petroleum, Petrochemicals and Advanced Materials, Chulalongkorn University, 254 Phayathai Road, Pathumwan, Bangkok 10330, Thailand

[d] Catalan Institution for Research and Advanced Studies (ICREA), Pg. Lluís Companys 23, 08010 Barcelona, Spain

KEYWORDS electroluminescent lamp, graphene, sensor, screen printing, breath control, smartphone-based sensing

ABSTRACT.

A screen-printed electroluminescent display with different sensing capabilities is presented. The sensing principle is based on the direct relationship between the light intensity of the lamp and the conductivity of the external layers. The proposed device is able to detect the ionic concentration of any conductive species. Using both top and bottom emission architectures, for the first time, a humidity sensor based on electroluminescent display functionalized by graphene oxide nanocomposite is introduced. In this regard, just by coupling the display to a smartphone camera sensor, its potential was expanded for automatically monitoring human respiration in real time. Besides, the research includes a responsive display in which the light is spatially turned on in response to pencil drawing or any other conductive media. The above-mentioned features together with the easiness of manufacturing and cost-effectiveness of this electroluminescent display can open up great opportunities to exploit it in sensing applications and point of care diagnosis.

INTRODUCTION

The growing and continuous demand for flexible optoelectronics[1-8] together with the evolution of wearable/portable electronics accessories have made possible that devices with good mechanical manipulation as folding, bending or rolling open up new opportunities for diverse applications[9-17]. In this perspective, alternating current electroluminescent (ACEL) displays are very promising due to their intrinsic ability of uniform light emission, low heat generation, flexible architecture and low power consumption[18-21]. Also, this type of devices can be easily fabricated by inexpensive screen-printing methods. So far, ACEL has been extensively used in

commercial applications such as black lighting, decorative lighting, panel display or even large-scale billboard[19, 22-24]. Nevertheless, the expansion of ACEL display technology toward the sensing field is still rather limited and have been barely exploited[25-26] representing, therefore, a big challenge for the scientific community.

Usually, to build a conventional ACEL display, transparent conductive materials on a transparent substrate are strictly required as a rear electrode in which the emitted light goes through the substrate located at the bottom[20, 27-29]. The transparent electrode produced from indium tin oxide (ITO) is typically used for this purpose. Alternatively, top-emission structure (TES) has been explored[19]. In TES architecture, the light from the phosphor layer is emitted directly through a top transparent conductive material, while the substrate is at the bottom (see Figure 1a). In contrast to bottom-emission structure (BES), this reversed architecture usually yields a higher brightness (under the same applied voltage) due to the shorter light path[19]. Besides, various substrates (e.g. paper, plastic or textile) can be chosen since there is no requisite for the substrate to be transparent[30-31]. By taking advantage of the different configurations, we envisioned that an ACEL display would be useful to create a versatile sensing platform. The light emission of an ACEL display mainly relies on the conductivities of the top conductive layer[32]. Hence, the change in conductance in the top layer of the ACEL display coming from an exposure of ions/charge carriers could alter the intensity of the emitted light. The direct relationship between the luminance and the conductivity could lead to sensing of a variety of conductive species, through the electroluminescence monitoring.

In this study, we engineered a powerful sensor based on ACEL display architecture lacking in the top electrode. This sensor is capable to detect and directly visualize the target analyte. To demonstrate its sensing ability, the ionic concentration of various water samples was monitored

as proof of concept. In addition, we took advantages of graphene oxide (GO) and its interesting properties in devices applications[33-35]. Using both TES and BES architectures, for the first time, a humidity sensor based on ACEL display functionalized by GO nanocomposite is introduced. Furthermore, we demonstrated the high-performance of the developed sensor as point-of-care (POC) device to monitor human breath which may be interesting for further applications.

RESULTS AND DISCUSSION

An ACEL lamp was fabricated using a screen-printing technique. The overall schematic of a lamp structure (5 x 5 cm) is shown in Figure 1a. For full fabrication of ACEL lamp with TES configuration, the process began with coating a layer of silver paste ink onto the substrate as the rear electrode, followed by a sequential coating of the dielectric layer. The phosphor was then coated on top of the dielectric layer. Finally, another layer of clear conductive ink was coated as the top electrode. As was mentioned above, in TES structure, the range of substrates is not limited to a transparent substrate; opaque flexible substrates varying from papers to commercial fabric can be used. As illustrated in Figure S1, the screen-printed electroluminescent lamp was fully achieved with the subsequent white light emission on different substrates (paper and plastic). Such a wide range of substrate selection may tune the resulting electroluminescence as well as the elasticity of the device platform.

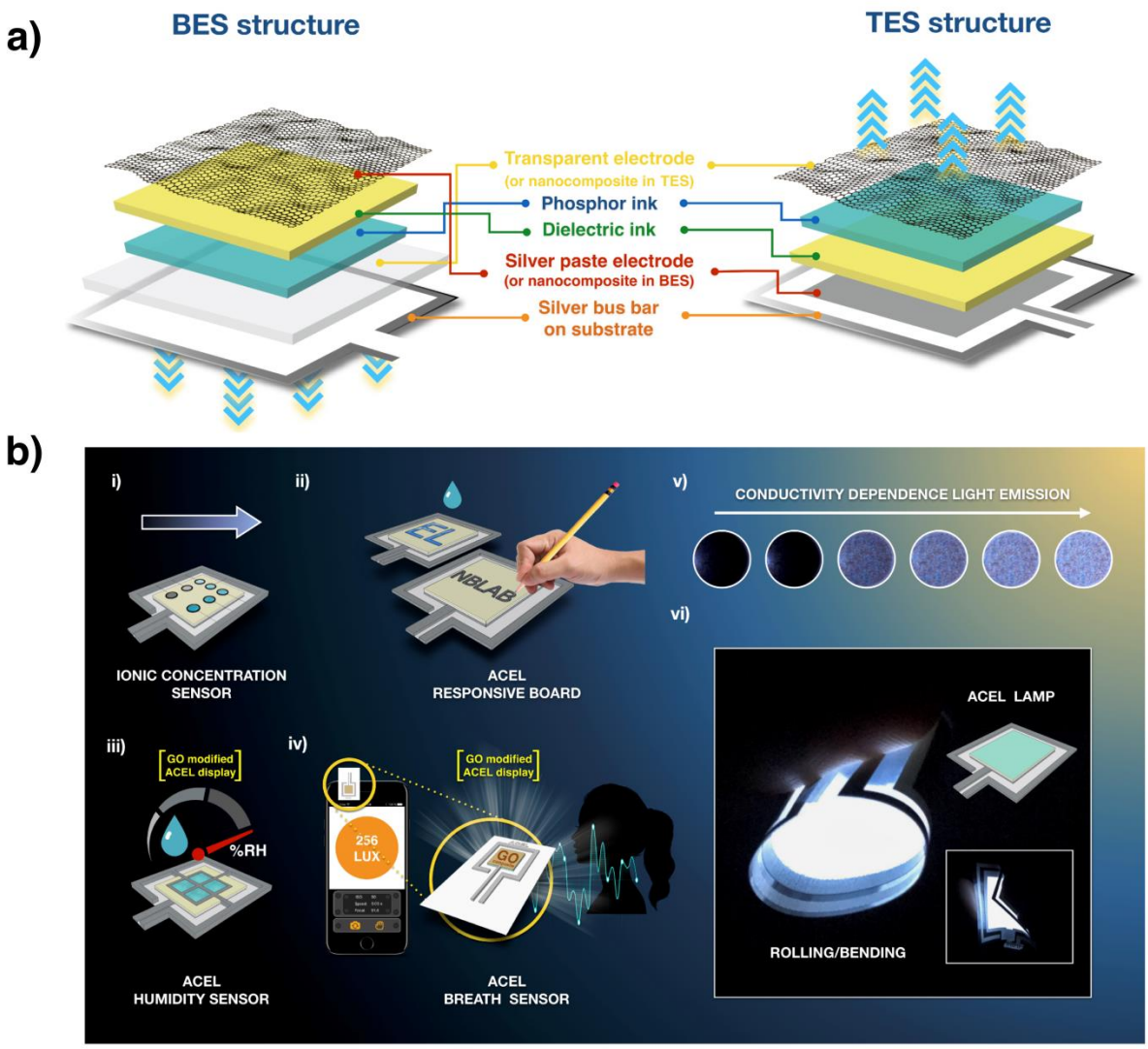

Figure 1. (a) Schematic image of alternating-current electroluminescent (ACEL) display with BES and TES architectures. (b) Schematic illustration of the ACEL display working concept to sense (i) ionic concentration, (ii) writable conductance (responsive display), (iii) relative humidity level, and (iv) human breathing. (v) Photographs of the ACEL display on exposure of NaCl solution having different ionic concentrations/conductivities. (vi) Photographs of the ACEL display under bending/rolling conditions.

Other than being just a simple light panel, this ACEL display offers promising applications. As proof of concept, various sensing platforms based on flexible ACEL display are developed and proposed (Figure 1b). Using the dependence between light emission and conductivity of ACEL display as a primary tool, a variety of sensing approaches were designed and applied. For instance, the sense of (i) ionic concentration/conductance allowing water sample analysis, (ii) writable conductance (responsive board), (iii) relative humidity level, and (iv) human breathing using a smartphone will be demonstrated in this work.

Fabrication of a multilayered ACEL display with TES configuration was further corroborated by scanning electron microscopy (SEM) cross-sectional image. As depicted in Figure 2a, the thickness of the silver paste electrode, dielectric layer, and phosphor layer are about 18 μm, 89 μm and 71 μm, respectively. Energy dispersive X-ray (SEM/EDX) analysis in line-scan mode was also performed to analyze the elemental constituent of each layer (Figure S2). A major component of phosphor layer was substantiated to be ZnS particles, while the subsequence layer of dielectric is made of $BaTiO_3$ particles. The individual layer surface morphology was also characterized by SEM (Figure S3). Illustrating in figure S3a is an irregular shape of silver particles, which is extensively deposited over the whole substrate surface. As displayed in figure S3b, the dielectric layer exhibited a very rough surface, consisting of dense $BaTIO_3$ particles. In addition, in Figure S3c, together with the cross-sectional image, the light emitting phosphor layer appeared as a smoother surface compared to the underlying dielectric layer. The large grain phosphor particles distributed evenly over the surface.

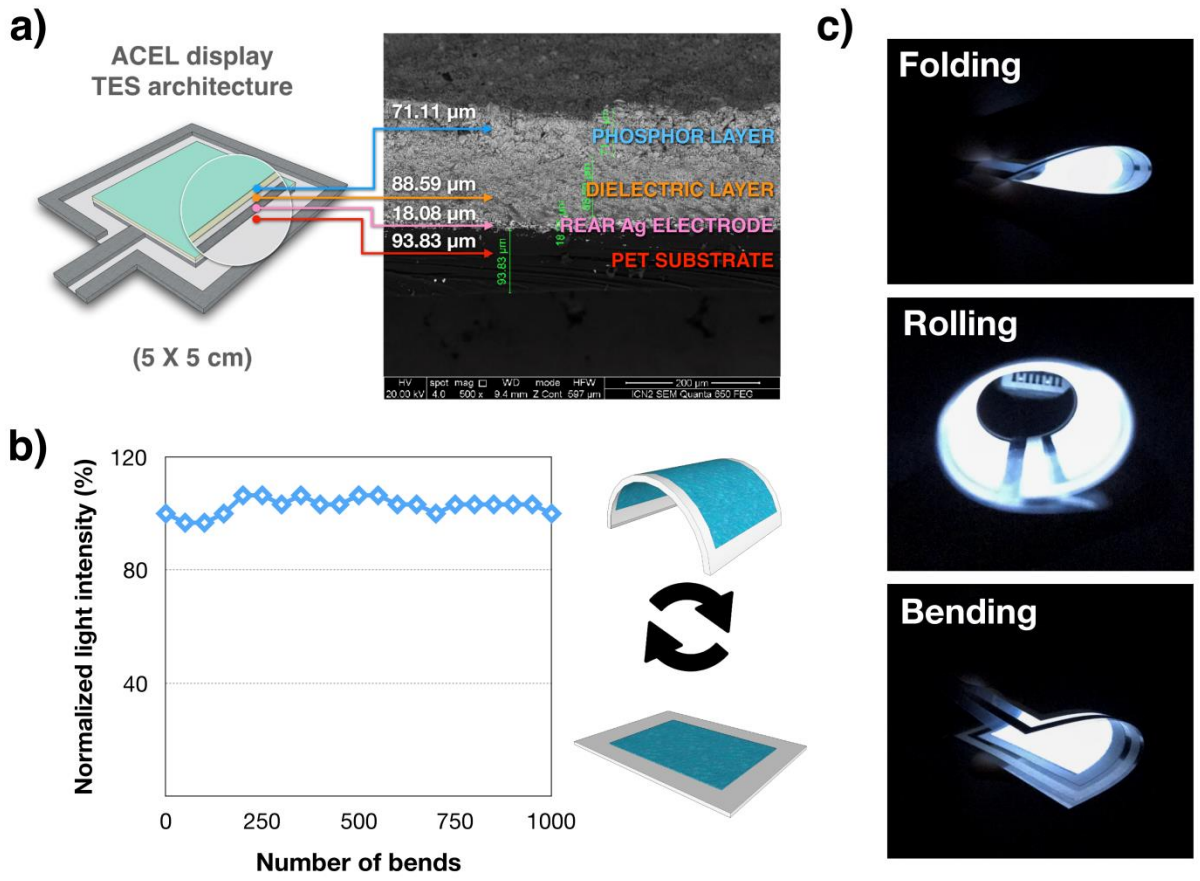

Figure 2. (a) Schematic representation and scanning electron microscopy (SEM) cross-sectional image of an ACEL display structure. (b) Normalized light intensity as a function of the number of bends (bending measurement procedure is shown). (c) Images of ACEL display (TES) with clear conductive ink fabricated on PET substrate under different mechanical deformation conditions.

To investigate the flexible and bendable ability of the electroluminescent display, the performance of the lamp in the presence of clear conductive ink electrode under bending condition was examined. The result from figure 2b shows that the emitted light intensity negligibly changed even after 1000 cycles of bending. The display could also be bent 180˚ or

rolled meanwhile maintaining the functionality (figure 2c). This demonstrates that the ACEL display held an excellent flexibility and durability to mechanical deformation.

Using the aforementioned TES ACEL lamp, a straightforward sensing platform based on electroluminescence was then sought to fabricate. In fact, the light emitted on an ACEL display is strongly affected by the conductivity of the materials over the phosphor layer. Hence, different conductivities would yield different electroluminescent intensities. To further investigate the relationship between conductivity and light emission, a solution of NaCl was carefully introduced on top of the phosphor layer of the ACEL display lacking in the top electrode. When the liquid solution spread over two electrodes that have the opposing phase of AC voltage (silver bus bar and underlying rear electrode), the light emission appears instantly (Figure S4, Movie S1). This phenomenon occurs because ions in the electrolyte solution can interconnect the electronic circuit, and then turns the light on. The light intensity as a function of solution conductivity was further studied. Various NaCl solutions having different ionic conductivities (MilliQ water ≈ 3.32 μS cm^{-1}; 1 mg L^{-1} ≈ 4.72 μS cm^{-1}; 5 mg L^{-1} ≈ 14.08 μS cm^{-1}; 10 mg L^{-1} ≈ 24.0 μS cm^{-1}; 100 mg L^{-1} ≈ 180.1 μS cm^{-1}; 1000 mg L^{-1} ≈ 1789 μS cm^{-1}) were tested. It should be noticed that printed-wax circles were used to define the sensing area onto the display in order to reduce large volume solution usage (Figure S5). Under the same applied voltage, the light intensity was proportional to the ionic concentration/conductivity of a saline solution (Figure 3a). This result indicates that the device can determine the ionic concentration/conductivity. Furthermore, using the light sensor embedded in a smartphone camera as an optical detection tool, the linear calibration between light intensity (lux) and logarithmic concentration of NaCl was established in the range of 1-100 mg L^{-1} (Figure 3b-c). It allows the quantitative evaluation of the ionic concentration. As proof of concept, water samples including milli-Q, distilled, and

tap water were inquired with the ACEL display. As expected, it was evident in the Figure 3d that tap and distilled water emit higher luminescence than milli-Q water owing to their larger dissolved ions concentration in the water.

As a result of this unique conductance-based light emission property, any conductive material could be visualized on this display. Thus, a simple responsive ACEL display with TES architecture has been exemplified in this work. Tap water or office pencil, for example, can be used as a conductive stylus to draw onto the surface of an ACEL panel. As indicated in Figure 3e and Movie S2, the light turns on instantaneously when this conductive media touched the electrode bar. Even though the electrode bar is inevitable, minimizing the bar size can make it invisible.

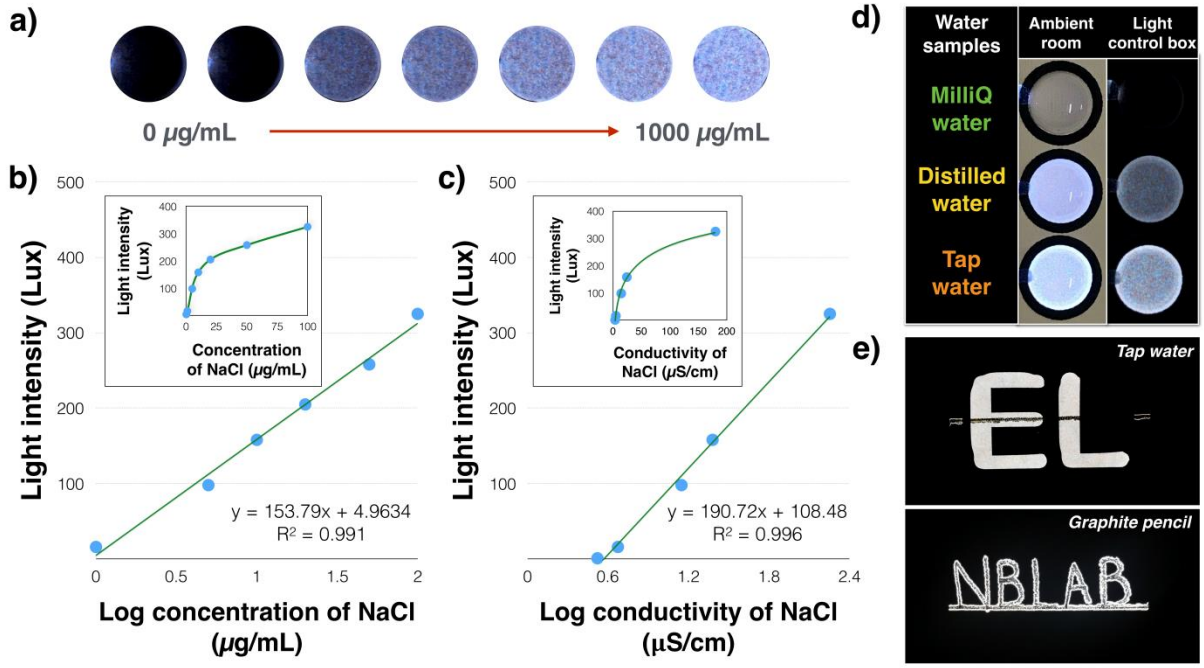

Figure 3. (a) Photographs of the ACEL display on exposure of NaCl solution having different ionic concentrations/conductivities. (b) The linear calibration of a plot between light intensity (lux) and log concentration of NaCl; and inset depicting the dependence of the light intensity vs.

concentration of NaCl. (c) The linear calibration of a plot between light intensity (lux) and log conductivity of NaCl; and inset depicting the dependence of the light intensity vs. conductivity of NaCl. (d) Photographs of the ACEL display testing with milli-Q, distilled, and tap water under ambient light (left) and light control box (right). (e) Photograph of alphabets on the responsive ACEL display written by tap water and graphite pencil.

We further broaden the potential of the electroluminescent platform to humidity sensing application which is of prime importance in various fields. Numerous publications for humidity monitoring have been reported over years. Most of them are based on capacitive and resistive change[36-43]. However, to the best of our knowledge, there is no report for humidity sensor based on electroluminescence. Therefore, a humidity sensor based on ACEL lamp using BES and TES structure functionalized by graphene oxide (GO)/Nafion nanocomposite as a sensitive material was applied here for the first time.

In this application, the sensing mechanism for an ACEL-based humidity sensor could be attributed to the proton conduction of nanocomposite formed between the 2D material (GO) and Nafion under a hydrated environment. In particular, GO derivative with oxygen-containing functional groups (−O−, −OH, and −COOH) possesses super-permeability to water molecules[44]. At low relative humidity (RH), the physisorbed water molecules on active site of GO (oxygen-containing functional groups) cannot move freely because of the restriction from double H−bond. For this reason, large energy is required for the hopping transfer of protons between adjacent active site, and therefore, results in strong electrical resistance. However, as %RH increases, the physisorbed water layer becomes mobile and behaves like a bulk liquid. Thus, the proton hopping mechanism between water molecules occurs in GO with charge transport taking place via the conductivity generated by a Grotthuss chain reaction, which in turn yields in an

increase of conductance[45-46]. Correspondingly, Nafion, a sulfonated fluoropolymer is also used to synergistically enhance ultrahigh proton conductivity in hydrated conditions[47-49]. This sulfonic acid hydrophilic group attached to the hydrophobic backbone in Nafion enables proton transport through hydrated ionic clusters and varies influentially with the humidity[48]. Moreover, the microstructures especially the percolated channel formed by these ionic clusters which may be sculptured by phase separation or colloidal packing is the key factor related to the proton conductivity of Nafion membrane[48, 50].

In this study, a larger light emission sensing area with surrounding square electrode was designed for both TES and BES to obtain maximum light intensity for humidity measurement. A simple drop-casting of the nanocomposite between GO and Nafion onto the phosphor layer of ACEL display raises interesting sensing applications. The nanocomposite based ACEL sensor was then characterized by SEM. SEM image of the composite device was then compared with those made with individual GO and Nafion. The formed GO film (figure S6a) exhibited a crumpled surface of nanosheet whereas Nafion film (figure S6b) displayed a smooth surface with several pores in the films. By contrast, the pore was not observed on the nanocomposite film covering ACEL display (figure S6c). The mixing of the Nafion with GO was responsible for the increase in the smooth surface with random nanoflakes of GO. The fabrication of the GO/Nafion nanocomposite was also confirmed by SEM/EDX analysis (figure S7), the F peak verified the presence of Nafion in GO films. It should be noted that the peaks of Zn, Al, S, Ba, and Ti could be ascribed to the elemental constituent of underlying layer of ACEL display. X-ray photon emission spectroscopy (XPS) was further used to confirm the surface of the sensor which corresponds only to the nanocomposite film. An overview of the XPS spectra is showed in figure S8A, where the characteristic peaks of GO and Nafion are identified. Moreover, it can be

observed at higher resolution (figure S8B) the typical peaks of C-C and C-O of the GO and the C-F peak of the Nafion. In addition, the thickness of the drop-casted film was found to be 1.488 μm in average, measured with stylus profilometer (figure S9).

To obtain the best sensitivity towards humidity, different proportions of GO and Nafion (1:9, 3:7, 5:5, 7:3 and 9:1) were then investigated at different relative humidity (RH), where RH was controlled in a custom-made chamber (figure 4a (i)) using vapor pressure from a set of saturated salt solution. As illustrated in Figure 4b, the light intensity response was inferior when GO was the major component (proportion) in the composite. The coverage of a phosphor layer with a brownish solution of GO can lead to a poor response. In contrast, when Nafion was in major proportion in the nanocomposite, higher sensitivity was achieved owing to its ultrahigh proton conductivity, especially for 3:7 ratio which exhibited maximum response. It is important to remark that the synergistic effect between GO and Nafion also resulted in higher light intensity response regarding humidity compared to the role of Nafion alone. The GO:Nafion composition of 3:7 was finally selected to obtain maximum efficiency for both TES and BES.

The performance of the sensor with TES configuration was firstly studied. It was obvious that no light is emitted at low RH. However, the light is automatically turned on in high humidity conditions (inset of Figure 4c (lower)). The exponential behavior of light intensity (lux) on the humidity is observed within studied range (inset of Figure 4c (upper)). This exponentially-sensitive behavior has been reported in several GO-based humidity sensors elsewhere, which might arise from mass loading effect of water adsorption at high RH[51-52]. Figure 4c shows the dependence of the logarithmic conductance-related light intensity (lux) on different RH values at room temperature. It is obvious that the logarithmic light intensity response increases linearly with the increment of %RH. Additionally, the humidity sensing capability of the ACEL display

with BES architecture was further investigated. In this way, an ACEL light panel was fabricated on a transparent electrode of ITO, following BES structure (see Figure 1a). However, a silver top-electrode was replaced by a sensitive layer of GO nanocomposite as is schematically shown in figure 4d. With this modified architecture, the direct feedback from humidity on nanocomposite layer would allow the phosphor layer on the opposite side to emit light. A light intensity response to different RH degrees is shown in Figure S10. A similar trend can be clearly observed, as in case of TES, whereby the light intensity increases exponentially with %RH. An enhanced sensitivity might be caused by the protective phosphor layer which is not hindered by the layer of GO nanocomposite. This humidity related light emission response holds a great promise to develop an innovative ACEL based humidity sensor for practical applications.

The capability of ACEL humidity sensor can be extended to further uses as point-of-care (POC) sensing device. Such a humidity-dependence light emission enables monitoring of human breathing through the moisture content in the exhaled air. The physical characteristics of the breath, such as breath frequency can provide helpful health condition information about pulmonary and cardiac symptoms[53-55].

In this experiment, the air exhaled was introduced using cylindrical mouthpiece connected to the custom-made chamber as illustrated in the experimental setup in the Figure 4a (ii). The response was then monitored through the light emission from ACEL sensor with TES architecture. The breath sensor performance of repeated exhale/inhale cycles is displayed in Figure S11. Once the breath was blown, the substantial response from light emission is rapidly detected. After the breath is off, the light emission was then gradually decreased. Different exhaled patterns including normal, deep and shallow breath were also reflected in different light intensity responses (dashed circle).

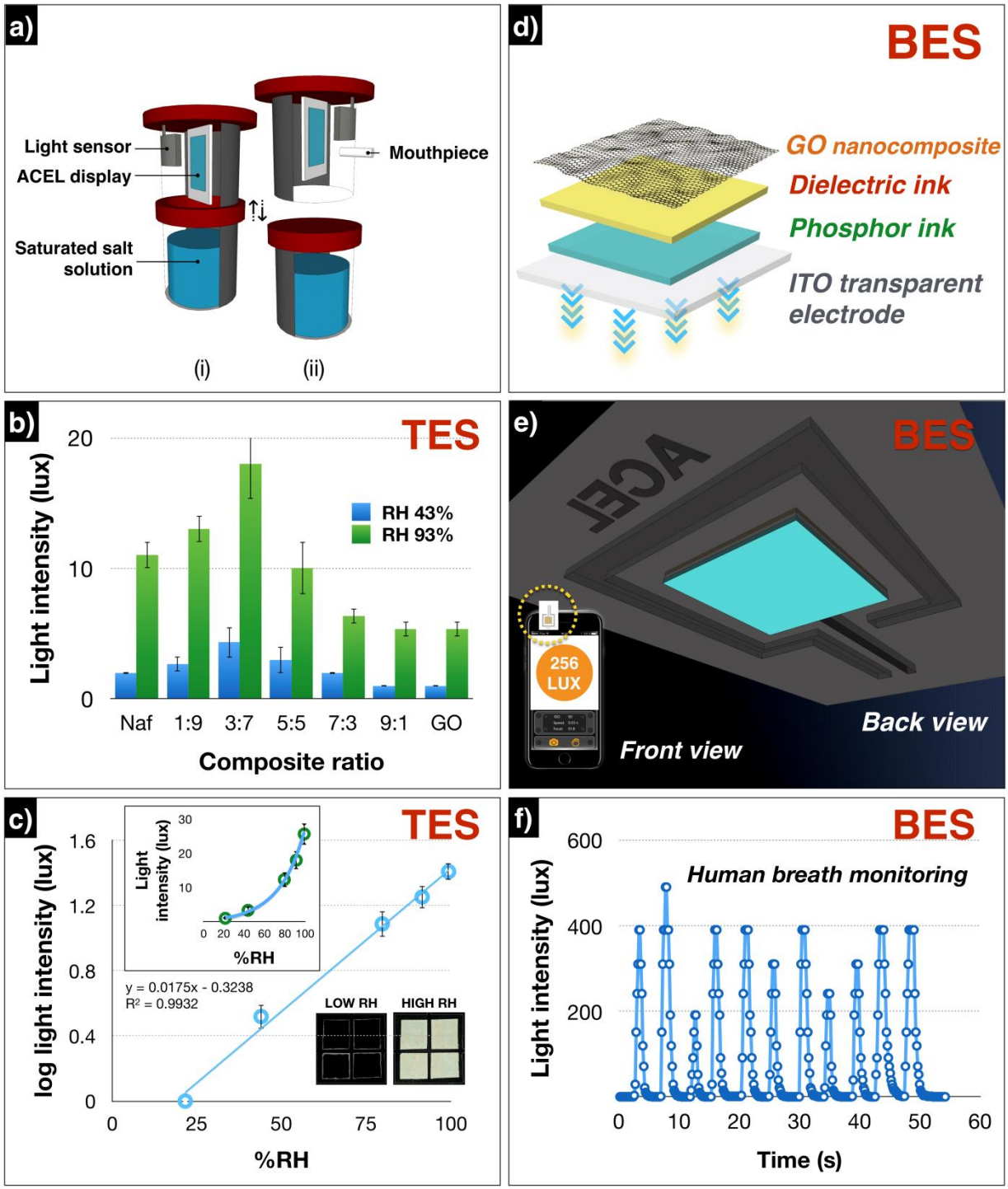

Figure 4. (a) Schematic illustration of a custom-made chamber for (i) controlling humidity and (ii) breath monitoring measurements. (b) Responses obtained for different GO / Nafion ratios

using ACEL with TES configuration. (c) A linear calibration plot between the logarithmic light intensity (lux) and %RH; and inset (upper) showing the exponential behavior between the light intensity response under different RH, (lower) real image results of an ACEL sensor upon exposure to different humidity levels. (d) Schematic image showing an ACEL sensor with BES architecture functionalized with GO nanocomposite. (e) Schematic illustration of the back view of ACEL sensor with BES and inset showing device arrangement with a smartphone. (f) The performance of an ACEL sensor with BES architecture for human breath monitoring.

The response and recovery times were further evaluated from single exhale/inhale cycles. As is observed in Figure S12, the sensor response to a breath could be as fast as 1s (time interval of the light sensor was limited at 1s), while the recovery time (defined as the time required to recover up to 90% of initial baseline) was varied depending on breathing patterns. For shallow and normal breathing, the recovery time was around 7s. However, in the case of deep breathing, the recovery time may take up to 12.5s (without applying any heat treatment). A huge difference between response and recovery time could be assigned to the generous hydrophilic functional moiety in GO and Nafion which required a longer time to desorb water molecules[56]. This experiment suggests that the developed breath monitoring sensor is capable to track the breathing frequency by a sensitive ACEL display.

To allow portability and simplicity for on-field POC testing, an ACEL humidity sensor integrated with the smartphone was then developed and demonstrated. Taking advantages of the BES configuration, the light emitted from the bottom of the ACEL sensor can be directly monitored through the light sensor embedded in a digital camera. As represented in Figure 4e, the back side of the ACEL display (1.3 × 1.3 cm) was attached to the front light sensor of a

smartphone. Clearly, the smartphone-based sensor exhibits a notable response towards human breathing (Figure 4f). Interestingly, both response and recovery time were estimated to be less than 1s. This ultrafast response/recovery time facilitates the detection of a broad range of respiratory rate in the patient. Although a clear electrode is mandatory for this architecture, an immediate and straightforward analysis was achieved without the need to use advanced equipment. A simple operation together with real-time monitoring enables it to use even by the untrained user. Based on this result, the smartphone-based ACEL sensor for human breath monitoring offers an excellent performance to become a smart tool for clinical diagnosis.

CONCLUSIONS

In summary, we have demonstrated the performance of a flexible ACEL display in sensing applications. The proposed device can be simply fabricated by a screen-printing method. In this platform, light emission occurs when conductive materials touched the sensing area of the phosphor layer, without requiring any top-transparent electrode. This conductance-dependence light emission enables the display to sense and visualize different water samples with various ionic concentrations. The direct response from pencil writing on ACEL display is also illustrated in this platform. For the first time, GO nanocomposite is integrated within an ACEL sensor and used to measure humidity. This innovative sensor can also be applied to human breath monitoring, where the light is automatically turned on when the exhaled air is in contact with the device. This flexible ACEL sensor holds a great potential for future advancement in wearable sensor technology in addition to other applications with interest for diagnostics as well as environmental monitoring, safety and security.

METHODS

All commercial reagents were of analytical grade and handled according to the material safety data sheets suggested by the suppliers. A flexible silver paste (C2131014D3), dielectric ink (D2070209P6), phosphor paste (C2150213D5), and clear conductive ink (C2100629D1) were purchased from Gwent group/SunChemical (Pontypool, UK). A water-based dispersion of single layer GO sheets (5 mg mL^{-1}) was purchased from Angstron Materials (OH, USA). 5% of Nafion 117 solution, NaCl, K_2CO_3, and KNO_3 were purchased from Sigma-Aldrich (Madrid, Spain). CH_3CO_2K and KCl were purchased from Panreac (Barcelona, Spain). All aqueous solutions were freshly prepared in ultrapure water produced using a Milli-Q system (>18.2 MΩ cm^{-1}) purchased from Millipore. SEM was performed through a Magellan 400L SEM High-Resolution SEM (FEI, Hillsboro, OR, USA). Cross-sectional SEM and EDX analysis were investigated by Quanta 650F Environmental SEM (FEI, Hillsboro, OR, USA). X-ray photoelectron spectroscopy (XPS) measurement was performed using a Phoibos 150 analyser (SPECS GmbH, Berlin, Germany). The thickness of the GO nanocomposite film was characterized by profilometer (Alpha Step D-500 Stylus Profiler, KLA-Tencor). A semi-automatic screen-printing machine DEK 248 (DEK International, Switzerland) was used for the screen-printing process. A wax printing was patterned with a Xerox ColorQube 8580 (Connecticut, USA) wax printer.

Fabrication of ACEL display: A polyethylene terephthalate (PET) film was used as the substrate; unless stated otherwise. Firstly, a flexible silver paste was printed directly onto PET substrate as the rear electrode and front bus-bar. Then, two layers of dielectric ink, a single layer of phosphor and clear conductor were sequentially printed onto the printed electrode. After each screen-printing layer, the screen-printed film was cured at 130℃ in a box oven for 10 minutes. For the use of ACEL in sensing applications, the prepared film was used without a clear

conductor screen-printing. A wax printing method was used to define circular sensing spots (diameter of 8 mm). The device was completed by drawing a straight line to connect the bus-bar and sensing area with a clear conductor. An AC voltage was powered by an EL inverter build in battery model UTF-EB900-4E (for DC 9.0V input).

Fabrication of GO/Nafion based humidity sensor: A 4-rectangular pattern was screen printed through a polyester screen directly on top of the ACEL display using flexible silver paste. To prepare the composite, 2.5 mg mL^{-1} GO solution (average lateral (x,y) and through-plane (z) dimension range of ≈ 500 nm and 1–1.2 nm, respectively, and C/O ratio about one unit (supplier's data)) was mixed with Nafion and sonicated for 1 hr. The prepared composite was carefully drop-casted onto an ACEL device and allowed to dry in the oven at 60℃ for 5 minutes.

The humidity measurement was conducted in a custom-made chamber consisting of an adaptable closed chamber, light sensor, and mouthpiece (Figure 4a). To achieve a certain level of humidity, RH was controlled by a series of saturated salt solution ranging low to high humidity level (CH_3CO_2K, K_2CO_3, NaCl, KCl, KNO_3) at room temperature. Each humidity level is kept constant for 30 min to obtain steady RH. The solution chamber was removed from the setup when a human breath is monitored. The breath was then blown directly to an ACEL sensor through a mouthpiece while the light emission is recorded.

ASSOCIATED CONTENT

Web enhanced Objects

Movie of light emission on ACEL display (Movie 1 ACEL)/responsive writable display (Movie 2 ACEL)

Supporting Information

Materials characterizations and additional experimental results (PDF)

AUTHOR INFORMATION

*** Corresponding Author**

E-mail: (A. M.) arben.merkoci@icn2.cat

E-mail: (O. C.) corawon@chula.ac.th

Notes

The authors declare no competing financial interest.

ACKNOWLEDGMENT

We acknowledge support from the Spanish MINECO under project MAT2014-52485-P. This work is also funded by the CERCA Programme / Generalitat de Catalunya. ICN2 is supported by the Severo Ochoa program from Spanish MINECO (Grant No. SEV-2013-0295). A.Y and O.C thank the Science Achievement Scholarship of Thailand (SAST), the Thailand Research Fund via the Research Team Promotion Grant (RTA6080002) and the Ratchadaphisaksomphot Endowment Fund of Chulalongkorn University. A.M. thanks Silver Merkoçi from Gwent Electronic Materials Ltd. / Sun Chemical for his inspiring discussions on the use of electroluminescent materials in sensing. R. A. acknowledges the financial support from the CONACYT (Mexico)

ABBREVIATIONS

ACEL, alternating-current electroluminescent; TES, top-emission structure; BES, bottom-emission structure; GO, graphene oxide.

REFERENCES

(1) Liu, J.; Xue, Y.; Wang, Z.; Xu, Z.-Q.; Zheng, C.; Weber, B.; Song, J.; Wang, Y.; Lu, Y.; Zhang, Y.; Bao, Q. Two-Dimensional CH3NH3PbI3 Perovskite: Synthesis and Optoelectronic Application. *ACS Nano* **2016,** *10* (3), 3536-3542, DOI: 10.1021/acsnano.5b07791.

(2) Bao, Q.; Loh, K. P. Graphene Photonics, Plasmonics, and Broadband Optoelectronic Devices. *ACS Nano* **2012,** *6* (5), 3677-3694, DOI: 10.1021/nn300989g.

(3) Oh, S. J.; Uswachoke, C.; Zhao, T.; Choi, J.-H.; Diroll, B. T.; Murray, C. B.; Kagan, C. R. Selective p- and n-Doping of Colloidal PbSe Nanowires To Construct Electronic and Optoelectronic Devices. *ACS Nano* **2015,** *9* (7), 7536-7544, DOI: 10.1021/acsnano.5b02734.

(4) Qin, J.; Qiu, G.; Jian, J.; Zhou, H.; Yang, L.; Charnas, A.; Zemlyanov, D. Y.; Xu, C.-Y.; Xu, X.; Wu, W.; Wang, H.; Ye, P. D. Controlled Growth of a Large-Size 2D Selenium Nanosheet and Its Electronic and Optoelectronic Applications. *ACS Nano* **2017**, DOI: 10.1021/acsnano.7b04786.

(5) Kwon, K. C.; Kim, C.; Le, Q. V.; Gim, S.; Jeon, J.-M.; Ham, J. Y.; Lee, J.-L.; Jang, H. W.; Kim, S. Y. Synthesis of Atomically Thin Transition Metal Disulfides for Charge Transport Layers in Optoelectronic Devices. *ACS Nano* **2015,** *9* (4), 4146-4155, DOI: 10.1021/acsnano.5b01504.

(6) Park, Y.; Ryu, B.; Oh, B.-R.; Song, Y.; Liang, X.; Kurabayashi, K. Biotunable Nanoplasmonic Filter on Few-Layer MoS2 for Rapid and Highly Sensitive Cytokine

Optoelectronic Immunosensing. *ACS Nano* **2017,** *11* (6), 5697-5705, DOI: 10.1021/acsnano.7b01162.

(7) Hu, G.; Albrow-Owen, T.; Jin, X.; Ali, A.; Hu, Y.; Howe, R. C. T.; Shehzad, K.; Yang, Z.; Zhu, X.; Woodward, R. I.; Wu, T.-C.; Jussila, H.; Wu, J.-B.; Peng, P.; Tan, P.-H.; Sun, Z.; Kelleher, E. J. R.; Zhang, M.; Xu, Y.; Hasan, T. Black phosphorus ink formulation for inkjet printing of optoelectronics and photonics. *Nature Communications* **2017,** *8* (1), 278, DOI: 10.1038/s41467-017-00358-1.

(8) Dong, H.; Wu, Z.; Jiang, Y.; Liu, W.; Li, X.; Jiao, B.; Abbas, W.; Hou, X. A Flexible and Thin Graphene/Silver Nanowires/Polymer Hybrid Transparent Electrode for Optoelectronic Devices. *ACS Applied Materials & Interfaces* **2016,** *8* (45), 31212-31221, DOI: 10.1021/acsami.6b09056.

(9) Kim, T.-H.; Lee, C.-S.; Kim, S.; Hur, J.; Lee, S.; Shin, K. W.; Yoon, Y.-Z.; Choi, M. K.; Yang, J.; Kim, D.-H.; Hyeon, T.; Park, S.; Hwang, S. Fully Stretchable Optoelectronic Sensors Based on Colloidal Quantum Dots for Sensing Photoplethysmographic Signals. *ACS Nano* **2017,** *11* (6), 5992-6003, DOI: 10.1021/acsnano.7b01894.

(10) Jinno, H.; Fukuda, K.; Xu, X.; Park, S.; Suzuki, Y.; Koizumi, M.; Yokota, T.; Osaka, I.; Takimiya, K.; Someya, T. Stretchable and waterproof elastomer-coated organic photovoltaics for washable electronic textile applications. *Nature Energy* **2017**, DOI: 10.1038/s41560-017-0001-3.

(11) Lee, H.; Kim, M.; Kim, I.; Lee, H. Flexible and Stretchable Optoelectronic Devices using Silver Nanowires and Graphene. *Advanced Materials* **2016,** *28* (22), 4541-4548, DOI: 10.1002/adma.201505559.

(12) Yi, F.; Wang, J.; Wang, X.; Niu, S.; Li, S.; Liao, Q.; Xu, Y.; You, Z.; Zhang, Y.; Wang, Z. L. Stretchable and Waterproof Self-Charging Power System for Harvesting Energy from Diverse Deformation and Powering Wearable Electronics. *ACS Nano* **2016,** *10* (7), 6519-6525, DOI: 10.1021/acsnano.6b03007.

(13) Cheng, Y.; Zhang, H.; Wang, R.; Wang, X.; Zhai, H.; Wang, T.; Jin, Q.; Sun, J. Highly Stretchable and Conductive Copper Nanowire Based Fibers with Hierarchical Structure for Wearable Heaters. *ACS Applied Materials & Interfaces* **2016,** *8* (48), 32925-32933, DOI: 10.1021/acsami.6b09293.

(14) Koo, J. H.; Jeong, S.; Shim, H. J.; Son, D.; Kim, J.; Kim, D. C.; Choi, S.; Hong, J.-I.; Kim, D.-H. Wearable Electrocardiogram Monitor Using Carbon Nanotube Electronics and Color-Tunable Organic Light-Emitting Diodes. *ACS Nano* **2017**, DOI: 10.1021/acsnano.7b04292.

(15) Choi, S.; Lee, H.; Ghaffari, R.; Hyeon, T.; Kim, D.-H. Recent Advances in Flexible and Stretchable Bio-Electronic Devices Integrated with Nanomaterials. *Advanced Materials* **2016,** *28* (22), 4203-4218, DOI: 10.1002/adma.201504150.

(16) Cheng, Y.; Wang, R.; Sun, J.; Gao, L. A Stretchable and Highly Sensitive Graphene-Based Fiber for Sensing Tensile Strain, Bending, and Torsion. *Advanced Materials* **2015,** *27* (45), 7365-7371, DOI: 10.1002/adma.201503558.

(17) Kim, J.; Shim, H. J.; Yang, J.; Choi, M. K.; Kim, D. C.; Kim, J.; Hyeon, T.; Kim, D.-H. Ultrathin Quantum Dot Display Integrated with Wearable Electronics. *Advanced Materials*, 1700217-n/a, DOI: 10.1002/adma.201700217.

(18) Park, J. H.; Lee, S. H.; Kim, J. S.; Kwon, A. K.; Park, H. L.; Han, S. D. White-electroluminescent device with ZnS:Mn, Cu, Cl phosphor. *Journal of Luminescence* **2007,** *126* (2), 566-570, DOI: https://doi.org/10.1016/j.jlumin.2006.10.012.

(19) Liang, G.; Hu, H.; Liao, L.; He, Y.; Ye, C. Highly Flexible and Bright Electroluminescent Devices Based on Ag Nanowire Electrodes and Top-Emission Structure. *Advanced Electronic Materials* **2017,** *3* (3), 1600535-n/a, DOI: 10.1002/aelm.201600535.

(20) Schrage, C.; Kaskel, S. Flexible and Transparent SWCNT Electrodes for Alternating Current Electroluminescence Devices. *ACS Applied Materials & Interfaces* **2009,** *1* (8), 1640-1644, DOI: 10.1021/am9002588.

(21) Torres Alonso, E.; Karkera, G.; Jones, G. F.; Craciun, M. F.; Russo, S. Homogeneously Bright, Flexible, and Foldable Lighting Devices with Functionalized Graphene Electrodes. *ACS Applied Materials & Interfaces* **2016,** *8* (26), 16541-16545, DOI: 10.1021/acsami.6b04042.

(22) Rack, P. D.; Holloway, P. H. The structure, device physics, and material properties of thin film electroluminescent displays. *Materials Science and Engineering: R: Reports* **1998,** *21* (4), 171-219, DOI: https://doi.org/10.1016/S0927-796X(97)00010-7.

(23) Haranath, D.; Shanker, V.; Vij, D. R. Electroluminescence. In *Handbook of Electroluminescent Materials*; Taylor & Francis: 2004.

(24) Cho, S. H.; Jo, S. S.; Hwang, I.; Sung, J.; Seo, J.; Jung, S.-H.; Bae, I.; Choi, J. R.; Cho, H.; Lee, T.; Lee, J. K.; Lee, T.-W.; Park, C. Extremely Bright Full Color Alternating Current Electroluminescence of Solution-Blended Fluorescent Polymers with Self-Assembled Block Copolymer Micelles. *ACS Nano* **2013,** *7* (12), 10809-10817, DOI: 10.1021/nn4040926.

(25) Berndt, K. W.; Lakowicz, J. R. Electroluminescent lamp-based phase fluorometer and oxygen sensor. *Analytical Biochemistry* **1992,** *201* (2), 319-325, DOI: https://doi.org/10.1016/0003-2697(92)90345-8.

(26) En-on, J.; Tuantranont, A.; Kerdcharoen, T.; Wongchoosuk, C. Flexible alternating current electroluminescent ammonia gas sensor. *RSC Advances* **2017,** *7* (27), 16885-16889, DOI: 10.1039/C7RA01318C.

(27) Wang, Z.-g.; Chen, Y.-f.; Li, P.-j.; Hao, X.; Liu, J.-b.; Huang, R.; Li, Y.-r. Flexible Graphene-Based Electroluminescent Devices. *ACS Nano* **2011,** *5* (9), 7149-7154, DOI: 10.1021/nn2018649.

(28) You, B.; Kim, Y.; Ju, B.-K.; Kim, J.-W. Highly Stretchable and Waterproof Electroluminescence Device Based on Superstable Stretchable Transparent Electrode. *ACS Applied Materials & Interfaces* **2017,** *9* (6), 5486-5494, DOI: 10.1021/acsami.6b14535.

(29) Wood, V.; Panzer, M. J.; Chen, J.; Bradley, M. S.; Halpert, J. E.; Bawendi, M. G.; Bulović, V. Inkjet-Printed Quantum Dot–Polymer Composites for Full-Color AC-Driven Displays. *Advanced Materials* **2009,** *21* (21), 2151-2155, DOI: 10.1002/adma.200803256.

(30) Sloma, M.; Janczak, D.; Wroblewski, G.; Mlozniak, A.; Jakubowska, M. Electroluminescent structures printed on paper and textile elastic substrates. *Circuit World* **2014,** *40* (1), 13-16, DOI: doi:10.1108/CW-10-2013-0037.

(31) Withnall, R.; Harris, P.; Silver, J.; Jones, S. 28.1: Invited Paper: Novel, Bright, Inorganic Electroluminescent Flexible Displays Comprising Ink Jet Printed Silver Back Electrodes. *SID Symposium Digest of Technical Papers* **2010,** *41* (1), 397-400, DOI: 10.1889/1.3500470.

(32) Kim, E. H.; Cho, S. H.; Lee, J. H.; Jeong, B.; Kim, R. H.; Yu, S.; Lee, T.-W.; Shim, W.; Park, C. Organic light emitting board for dynamic interactive display. *Nature Communications* **2017,** *8*, 14964, DOI: 10.1038/ncomms14964

https://www.nature.com/articles/ncomms14964#supplementary-information.

(33) Morales-Narváez, E.; Merkoçi, A. Graphene Oxide as an Optical Biosensing Platform. *Advanced Materials* **2012,** *24* (25), 3298-3308, DOI: 10.1002/adma.201200373.

(34) Morales-Narváez, E.; Sgobbi, L. F.; Machado, S. A. S.; Merkoçi, A. Graphene-encapsulated materials: Synthesis, applications and trends. *Progress in Materials Science* **2017,** *86* (Supplement C), 1-24, DOI: https://doi.org/10.1016/j.pmatsci.2017.01.001.

(35) Chałupniak, A.; Merkoçi, A. Toward integrated detection and graphene-based removal of contaminants in a lab-on-a-chip platform. *Nano Research* **2017,** *10* (7), 2296-2310, DOI: 10.1007/s12274-016-1420-3.

(36) Li, N.; Chen, X.; Chen, X.; Ding, X.; Zhao, X. Ultrahigh humidity sensitivity of graphene oxide combined with Ag nanoparticles. *RSC Advances* **2017,** *7* (73), 45988-45996, DOI: 10.1039/C7RA06959F.

(37) Miyoshi, Y.; Miyajima, K.; Saito, H.; Kudo, H.; Takeuchi, T.; Karube, I.; Mitsubayashi, K. Flexible humidity sensor in a sandwich configuration with a hydrophilic porous membrane. *Sensors and Actuators B: Chemical* **2009,** *142* (1), 28-32, DOI: https://doi.org/10.1016/j.snb.2009.07.014.

(38) Zampetti, E.; Pantalei, S.; Pecora, A.; Valletta, A.; Maiolo, L.; Minotti, A.; Macagnano, A.; Fortunato, G.; Bearzotti, A. Design and optimization of an ultra thin flexible capacitive

humidity sensor. *Sensors and Actuators B: Chemical* **2009,** *143* (1), 302-307, DOI: https://doi.org/10.1016/j.snb.2009.09.004.

(39) Zhang, D.; Tong, J.; Xia, B.; Xue, Q. Ultrahigh performance humidity sensor based on layer-by-layer self-assembly of graphene oxide/polyelectrolyte nanocomposite film. *Sensors and Actuators B: Chemical* **2014,** *203* (Supplement C), 263-270, DOI: https://doi.org/10.1016/j.snb.2014.06.116.

(40) Han, J.-W.; Kim, B.; Li, J.; Meyyappan, M. Carbon Nanotube Based Humidity Sensor on Cellulose Paper. *The Journal of Physical Chemistry C* **2012,** *116* (41), 22094-22097, DOI: 10.1021/jp3080223.

(41) Kuang, Q.; Lao, C.; Wang, Z. L.; Xie, Z.; Zheng, L. High-Sensitivity Humidity Sensor Based on a Single SnO2 Nanowire. *Journal of the American Chemical Society* **2007,** *129* (19), 6070-6071, DOI: 10.1021/ja070788m.

(42) Yu, H.-W.; Kim, H. K.; Kim, T.; Bae, K. M.; Seo, S. M.; Kim, J.-M.; Kang, T. J.; Kim, Y. H. Self-Powered Humidity Sensor Based on Graphene Oxide Composite Film Intercalated by Poly(Sodium 4-Styrenesulfonate). *ACS Applied Materials & Interfaces* **2014,** *6* (11), 8320-8326, DOI: 10.1021/am501151v.

(43) Zhou, G.; Byun, J.-H.; Oh, Y.; Jung, B.-M.; Cha, H.-J.; Seong, D.-G.; Um, M.-K.; Hyun, S.; Chou, T.-W. Highly Sensitive Wearable Textile-Based Humidity Sensor Made of High-Strength, Single-Walled Carbon Nanotube/Poly(vinyl alcohol) Filaments. *ACS Applied Materials & Interfaces* **2017,** *9* (5), 4788-4797, DOI: 10.1021/acsami.6b12448.

(44) Nair, R. R.; Wu, H. A.; Jayaram, P. N.; Grigorieva, I. V.; Geim, A. K. Unimpeded Permeation of Water Through Helium-Leak–Tight Graphene-Based Membranes. *Science* **2012,** *335* (6067), 442-444, DOI: 10.1126/science.1211694.

(45) Bi, H.; Yin, K.; Xie, X.; Ji, J.; Wan, S.; Sun, L.; Terrones, M.; Dresselhaus, M. S. Ultrahigh humidity sensitivity of graphene oxide. *Scientific Reports* **2013,** *3*, 2714, DOI: 10.1038/srep02714

https://www.nature.com/articles/srep02714#supplementary-information.

(46) Karim, M. R.; Hatakeyama, K.; Matsui, T.; Takehira, H.; Taniguchi, T.; Koinuma, M.; Matsumoto, Y.; Akutagawa, T.; Nakamura, T.; Noro, S.-i.; Yamada, T.; Kitagawa, H.; Hayami, S. Graphene Oxide Nanosheet with High Proton Conductivity. *Journal of the American Chemical Society* **2013,** *135* (22), 8097-8100, DOI: 10.1021/ja401060q.

(47) O'Dea, J. R.; Economou, N. J.; Buratto, S. K. Surface Morphology of Nafion at Hydrated and Dehydrated Conditions. *Macromolecules* **2013,** *46* (6), 2267-2274, DOI: 10.1021/ma302399e.

(48) Liu, L.; Chen, W.; Li, Y. An overview of the proton conductivity of nafion membranes through a statistical analysis. *Journal of Membrane Science* **2016,** *504* (Supplement C), 1-9, DOI: https://doi.org/10.1016/j.memsci.2015.12.065.

(49) Kreuer, K.-D.; Dippel, T.; Meyer, W.; Maier, J. Nafion® Membranes: Molecular Diffusion, Proton Conductivity and Proton Conduction Mechanism. *MRS Proceedings* **2011,** *293*, DOI: 10.1557/PROC-293-273.

(50) Sumner, J. J.; Creager, S. E.; Ma, J. J.; DesMarteau, D. D. Proton Conductivity in Nafion® 117 and in a Novel Bis[(perfluoroalkyl)sulfonyl]imide Ionomer Membrane. *Journal of The Electrochemical Society* **1998,** *145* (1), 107-110, DOI: 10.1149/1.1838220.

(51) Xuan, W.; He, M.; Meng, N.; He, X.; Wang, W.; Chen, J.; Shi, T.; Hasan, T.; Xu, Z.; Xu, Y.; Luo, J. K. Fast Response and High Sensitivity ZnO/glass Surface Acoustic Wave Humidity Sensors Using Graphene Oxide Sensing Layer. *Scientific Reports* **2014,** *4*, 7206, DOI: 10.1038/srep07206

https://www.nature.com/articles/srep07206#supplementary-information.

(52) Borini, S.; White, R.; Wei, D.; Astley, M.; Haque, S.; Spigone, E.; Harris, N.; Kivioja, J.; Ryhänen, T. Ultrafast Graphene Oxide Humidity Sensors. *ACS Nano* **2013,** *7* (12), 11166-11173, DOI: 10.1021/nn404889b.

(53) Yasuma, F.; Hayano, J.-i. Respiratory Sinus Arrhythmia: Why Does the Heartbeat Synchronize With Respiratory Rhythm? *Chest* **2004,** *125* (2), 683-690, DOI: https://doi.org/10.1378/chest.125.2.683.

(54) Bates, J.; Schmalisch, G.; Filbrun, D.; Stocks, J. Tidal breath analysis for infant pulmonary function testing. ERS/ATS Task Force on Standards for Infant Respiratory Function Testing. European Respiratory Society/American Thoracic Society. *European Respiratory Journal* **2000,** *16* (6), 1180-1192.

(55) Du, B.; Yang, D.; She, X.; Yuan, Y.; Mao, D.; Jiang, Y.; Lu, F. MoS2-based all-fiber humidity sensor for monitoring human breath with fast response and recovery. *Sensors and*

Actuators B: Chemical **2017,** *251* (Supplement C), 180-184, DOI: https://doi.org/10.1016/j.snb.2017.04.193.

(56) Ghosh, S.; Ghosh, R.; Kumar Guha, P.; Bhattacharyya, T. K. Enhanced Proton Conductivity of Graphene Oxide/Nafion Composite Material in Humidity Sensing Application. *IEEE Transactions on Nanotechnology* **2016,** *15* (5), 782-790, DOI: 10.1109/TNANO.2016.2580739.

GRAPHICAL TABLE OF CONTENT